Myocardial T1 Mapping: Techniques and Potential Applications[1]

Jeremy R. Burt, MD[2]
Stefan L. Zimmerman, MD
Ihab R. Kamel, MD, PhD
Marc Halushka, MD, PhD
David A. Bluemke, MD, PhD

Abbreviations: ECG = electrocardiograph, ECM = extracellular matrix, ECV = extracellular volume fraction, IR = inversion recovery, LL = Look-Locker, MOLLI = modified Look-Locker inversion-recovery, PSIR = phase-sensitive inversion-recovery, ShMOLLI = shortened modified Look-Locker inversion-recovery, TI = inversion time

RadioGraphics 2014; 34:377–395

Published online 10.1148/rg.342125121

Content Codes: CA MR

[1]From the Russell H. Morgan Department of Radiology and Radiological Sciences (J.R.B., S.L.Z., I.R.K., D.A.B.) and Department of Pathology (M.H.), Johns Hopkins University School of Medicine, Baltimore, Md; and Radiology and Imaging Sciences, Clinical Center, and National Institute of Biomedical Imaging and Bioengineering, National Institutes of Health, 10 Center Dr, Room 1C355, Bethesda, MD 20892 (D.A.B.). Presented as an education exhibit at the 2011 RSNA Annual Meeting. Received May 21, 2012; revision requested June 20 and received December 24; final version accepted May 15, 2013. J.R.B. supported by an RSNA 2011 Silver Anniversary Campaign Pacesetters Research Fellow Grant (number RF1106). The other authors have no financial relationships to disclose. **Address correspondence to** D.A.B. (e-mail: *bluemked@mail.nih.gov*).

[2]Current address: Radiology Specialists of Florida, Florida Hospital, Orlando, Fla.

TEACHING POINTS

See last page

Myocardial fibrosis is a common endpoint in a variety of cardiac diseases and a major independent predictor of adverse cardiac outcomes. Short of histopathologic analysis, which is limited by sampling bias, most diagnostic modalities are limited in their depiction of myocardial fibrosis. Cardiac magnetic resonance (MR) imaging has the advantage of providing detailed soft-tissue characterization, and a variety of novel quantification methods have further improved its usefulness. Contrast material–enhanced cardiac MR imaging depends on differences in signal intensity between regions of scarring and adjacent normal myocardium. Diffuse myocardial fibrosis lacks these differences in signal intensity. Measurement of myocardial T1 times (T1 mapping) with gadolinium-enhanced inversion recovery–prepared sequences may depict diffuse myocardial fibrosis and has good correlation with ex vivo fibrosis content. T1 mapping calculates myocardial T1 relaxation times with image-based signal intensities and may be performed with standard cardiac MR imagers and radiologic workstations. Myocardium with diffuse fibrosis has greater retention of contrast material, resulting in T1 times that are shorter than those in normal myocardium. Early studies have suggested that diffuse myocardial fibrosis may be distinguished from normal myocardium with T1 mapping. Large multicenter studies are needed to define the role of T1 mapping in developing prognoses and therapeutic assessments. However, given its strengths as a noninvasive method for direct quantification of myocardial fibrosis, T1 mapping may eventually play an important role in the management of cardiac disease.

Introduction

The normal myocardium includes a network of cardiac cells embedded within mainly fibrillar collagen. This collagen matrix plays an essential role in giving strength to the heart, as well as creating an intercellular communication grid. Increased myocardial collagen deposition is the common endpoint for a wide variety of cardiomyopathies and results in abnormal myocardial stiffness and contractility, which leads to progression of heart failure and disruption of the intercellular communication grid and which, in turn, may lead to malignant arrhythmias and sudden death. Indeed, multiple clinical studies have shown fibrosis to be a major independent predictor of adverse cardiac outcomes (1–4).

Teaching Point

Table 1: Cardiac Diseases that Cause Myocardial Fibrosis

Diseases that Cause Reactive Interstitial Fibrosis
Aging, hypertension, diabetes, acute or chronic ischemia, valvular disorders, nonischemic dilated cardiomyopathy, rejection of a transplanted heart, hypertrophic cardiomyopathy, arrhythmogenic right ventricular cardiomyopathy, sarcoidosis, systemic lupus erythematosus, systemic sclerosis, Chagas disease, chronic renal insufficiency
Diseases that Cause Infiltrative Interstitial Fibrosis
Amyloidosis, Anderson-Fabry disease
Diseases that Cause Replacement Fibrosis
Ischemia, infarction, sarcoidosis, chronic renal insufficiency, myocarditis, toxic cardiomyopathies, plus all causes of reactive and infiltrative interstitial fibrosis

Source.—References 9–11, 14, 15, 19–31.

Historically, myocardial fibrosis was not useful as a clinical marker because the only available method for assessment was invasive endomyocardial biopsy, which was seldom performed. Even in those who undergo endomyocardial biopsy, results are limited by sampling bias (5). More recently, investigators have sought a noninvasive method to distinguish fibrotic myocardium from normal myocardium. Cardiac magnetic resonance (MR) imaging has the advantage of detailed soft-tissue characterization. A variety of novel methods of quantification have further improved its usefulness. Measurement of myocardial longitudinal relaxation time (T1 mapping) with gadolinium contrast material–enhanced inversion recovery (IR)–prepared sequences has emerged as a novel approach for possible noninvasive quantification of myocardial fibrosis. In this article, T1 mapping of diffuse interstitial fibrosis of the myocardium is discussed.

Pathogenesis of Myocardial Fibrosis

The extracellular matrix (ECM) is an essential component of the healthy heart and functions to anchor cardiac muscle cells, regulate tissue mechanics, and store growth factors (6–8). Normally, the ECM and fibrillar collagen network form only 6% and 2%–4%, respectively, of the structural space within the heart (9). An increased amount of collagen (fibrosis) in the myocardial tissue results from altered collagen turnover, in which net collagen deposition exceeds net collagen breakdown. Myocardial fibrosis increases with age (10). Although it is not entirely understood, after an initiating factor (eg, a toxin or mechanical injury), a cascade of chemokines, cytokines, and neurohormonal factors lead to local cell activation and collagen synthesis (11,12). Matrix metalloproteinases also play a key role in the development of myocardial fibrosis, which may be regionally distributed in the form of a scar or be more diffuse, depending on the underlying cause (13,14). In general, myocardial fibrosis is classified as replacement or interstitial fibrosis.

Replacement fibrosis is caused by the replacement of damaged or necrotic cells by plexiform fibrosis and is only seen when the integrity of the cell wall is affected (15). Both regional and diffuse patterns of replacement fibrosis may be present, depending on the underlying cause. The most common cause of replacement fibrosis is scarring from myocardial infarction. Other conditions associated with replacement fibrosis include hypertrophic cardiomyopathy, sarcoidosis, myocarditis, chronic renal insufficiency, and toxic cardiomyopathies (16,17). Late gadolinium contrast enhancement at cardiac MR imaging is a validated, noninvasive way to identify replacement fibrosis (18).

In general, interstitial fibrosis is diffuse, and its subtypes include reactive and infiltrative interstitial fibrosis. Reactive fibrosis is present in a variety of common conditions, including aging and hypertension (Table 1). It is caused by an increase in collagen production and deposition by stimulated myofibroblasts, which is thought to result from alterations in metabolism, activation of the renin-aldosterone-angiotensin system, and oxidative injury and usually results in diffuse collagen deposition in the myocardial interstitium (31,32). Infiltrative fibrosis is much more rare and is caused by progressive deposition of insoluble proteins or glycosphingolipids in the interstitium. Examples of infiltrative fibrosis include amyloidosis and Anderson-Fabry disease (27,28). Eventually, both interstitial and infiltrative fibrosis lead to cardiomyocyte apoptosis and replacement fibrosis (31).

In the heart, collagen remodeling plays an essential role in the development of a variety of cardiomyopathies and is always present in end-stage heart failure (33). Patients with increased myo-

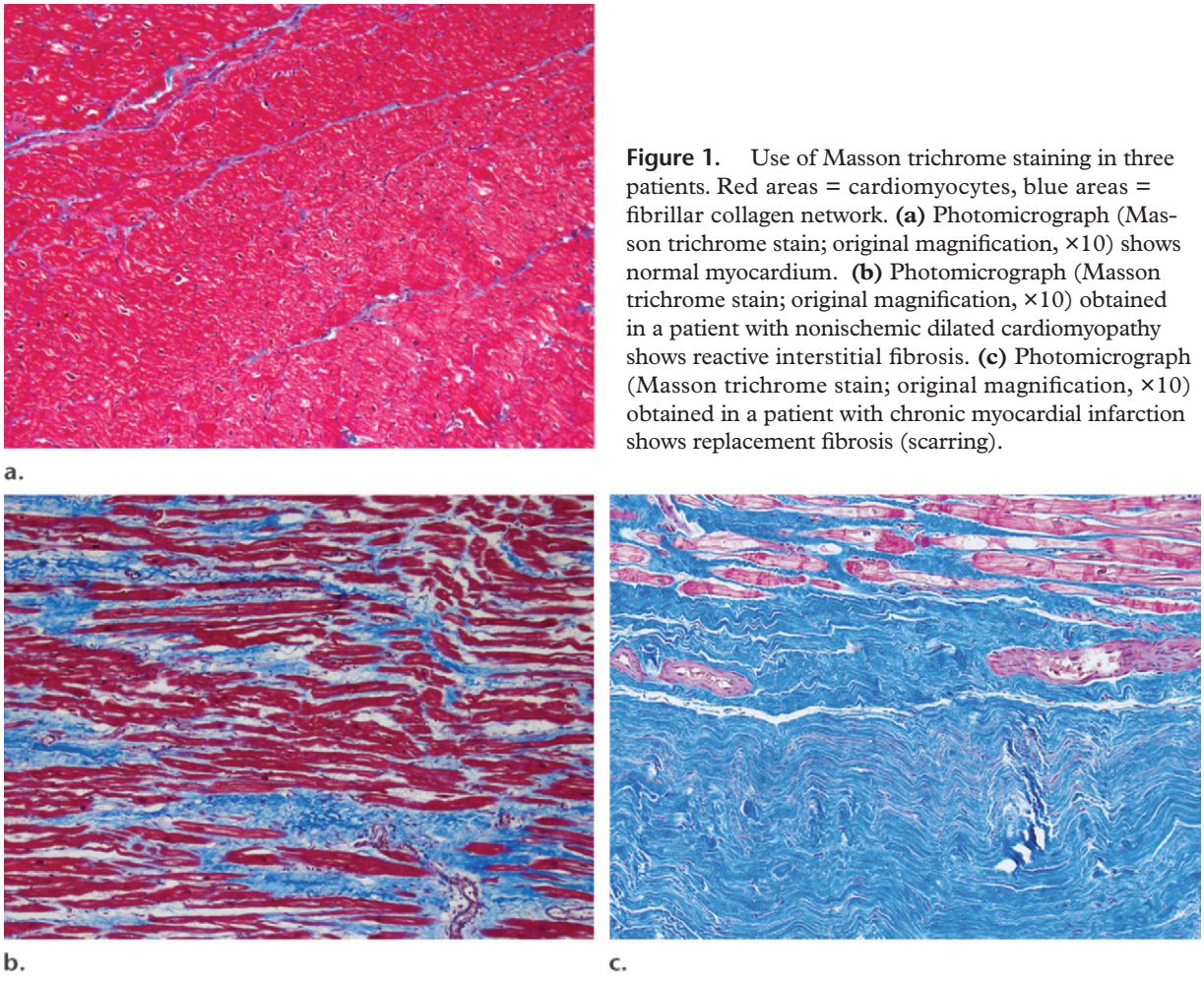

Figure 1. Use of Masson trichrome staining in three patients. Red areas = cardiomyocytes, blue areas = fibrillar collagen network. **(a)** Photomicrograph (Masson trichrome stain; original magnification, ×10) shows normal myocardium. **(b)** Photomicrograph (Masson trichrome stain; original magnification, ×10) obtained in a patient with nonischemic dilated cardiomyopathy shows reactive interstitial fibrosis. **(c)** Photomicrograph (Masson trichrome stain; original magnification, ×10) obtained in a patient with chronic myocardial infarction shows replacement fibrosis (scarring).

cardial collagen deposition have increased mortality, which is linked to sudden cardiac death, arrhythmias, and heart failure (5,7,34,35). Findings from animal and clinical studies indicate that diastolic function is initially affected and followed by deterioration of systolic function (31). Unlike replacement fibrosis, interstitial fibrosis may be reversible and is a target for treatment (36,37).

Assessment of Fibrosis

Endomyocardial biopsy—in which a small (<1 mm^3) sample is obtained with biopsy forceps, typically from the right ventricular side of the distal myocardial septum during catheterization of the right side of the heart—is the principle method for diagnosing myocardial fibrosis. The sample of myocardium is evaluated with Masson trichrome staining (Fig 1). Quantitative morphometry with picrosirius red under polarized light may be used to quantify absolute collagen volume fraction. Because of the invasive nature of this technique and the potential for complications and sampling errors, which limit diagnostic accuracy and reproducibility, other diagnostic methods are being investigated (5). Ideally, an accurate noninvasive method would allow early detection of disease, accurate prognostication, and targeted guidance of treatment without the risks associated with invasive methods. Cardiac MR imaging has the potential to fulfill these criteria and provide a comprehensive cardiac assessment with detailed information about cardiac anatomy and function. In contrast to endomyocardial biopsy, sampling errors may be avoided with cardiac MR imaging by assessing the degree of fibrosis throughout the entire left ventricular myocardium.

Teaching Point

Background of T1 Mapping

What Is Myocardial T1 Mapping?

T1 mapping consists of quantifying the T1 relaxation time of a tissue by using analytical expressions of image-based signal intensities. A fundamental principal of MR imaging is that the signal intensity of pixels is based on the relaxation of hydrogen nuclei protons in a static magnetic field (38). The T1 relaxation times between two tissues vary substantially. Edema, fat infiltration, and fibrosis also cause differences in T1 relaxivity. In some settings, the intrinsic T1 time of a tissue

Teaching Point

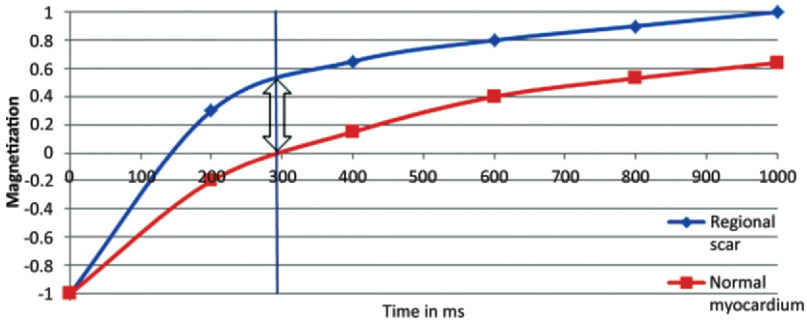

Figure 2. Graph shows the relaxation times of myocardium and focal scarring. In this example, maximal contrast (arrow) between regional scarring (blue line) and normal myocardium (red line) is achieved with an inversion time of 290 msec (vertical line).

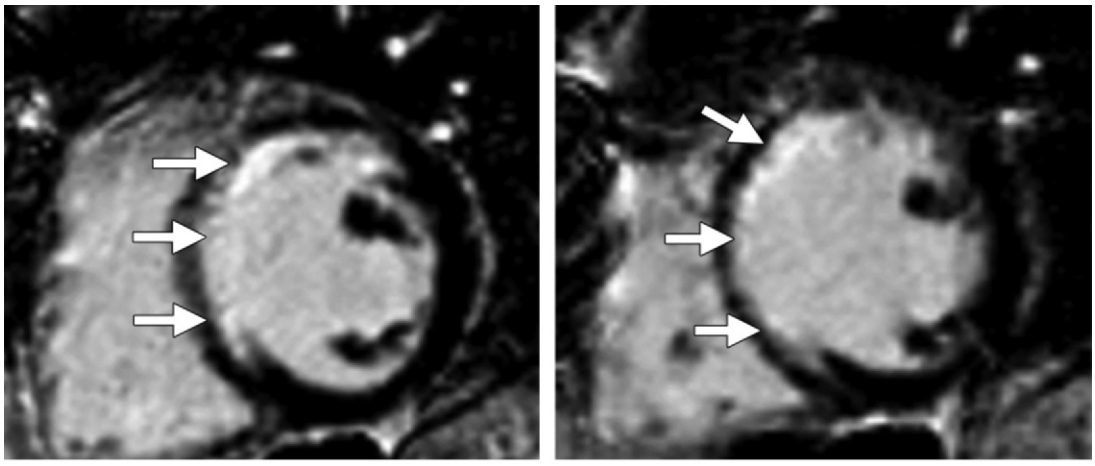

a. **b.**

Figure 3. Replacement fibrosis in a patient with a history of left anterior descending artery occlusion. Short-axis delayed contrast-enhanced phase-sensitive inversion-recovery (PSIR) MR images obtained at 1.5 T show regional subendocardial scarring (replacement fibrosis) in the septum and anteroseptal wall (arrows).

may act as a marker for the extent of myocardial disease (39,40). Specific IR-prepared cardiac MR imaging sequences are used to determine the rate of recovery of longitudinal magnetization (the T1 time).

T1 Mapping and Delayed Myocardial Enhancement

After intravenous administration of a gadolinium chelate contrast agent, myocardium-containing fibrosis demonstrates prolonged washout of the contrast agent, a finding related to decreased density of capillaries within the scar tissue and an increased extracellular volume of distribution (41). An increased concentration of gadolinium relaxes the adjacent protons much faster than usual, causing T1 shortening (an area of high signal intensity) on IR-prepared images (42). The difference in signal intensity between normal myocardium and scar tissue is enhanced by selecting an inversion time that nulls the signal from noninfarcted areas of myocardium (Fig 2).

The extent of collagen deposition within the myocardium varies depending on the type and severity of the cardiac disease. Focal scarring refers to an area of replacement fibrosis that is seen as regional late gadolinium enhancement at cardiac MR imaging (Fig 3). On the other hand, diffuse fibrosis is indicative of interstitial fibrosis at histopathologic analysis that is not seen at late gadolinium-enhanced cardiac MR imaging. The use of late gadolinium-enhanced cardiac MR imaging to depict focal scarring depends on visual differences in signal intensity between regions of scarring and adjacent normal myocardium. On standard delayed contrast-enhanced IR-prepared (delayed myocardial-enhanced) images, diffuse fibrosis lacks these differences in signal intensity and may not be visually distinguished from normal myocardium. In addition, in cases of uniform dispersion of interstitial fibrosis, the use of inversion pulses with standard delayed contrast-enhanced cardiac MR imaging techniques uniformly suppresses the entire myocardium despite the presence of retained gadolinium contrast material (Fig 4).

T1 mapping overcomes these limitations by measuring the intrinsic T1 time (in msec) of the tissue being evaluated. Other aspects of standard contrast-enhanced IR-prepared imaging that may be difficult to standardize—such as optimized window leveling, inadvertent use

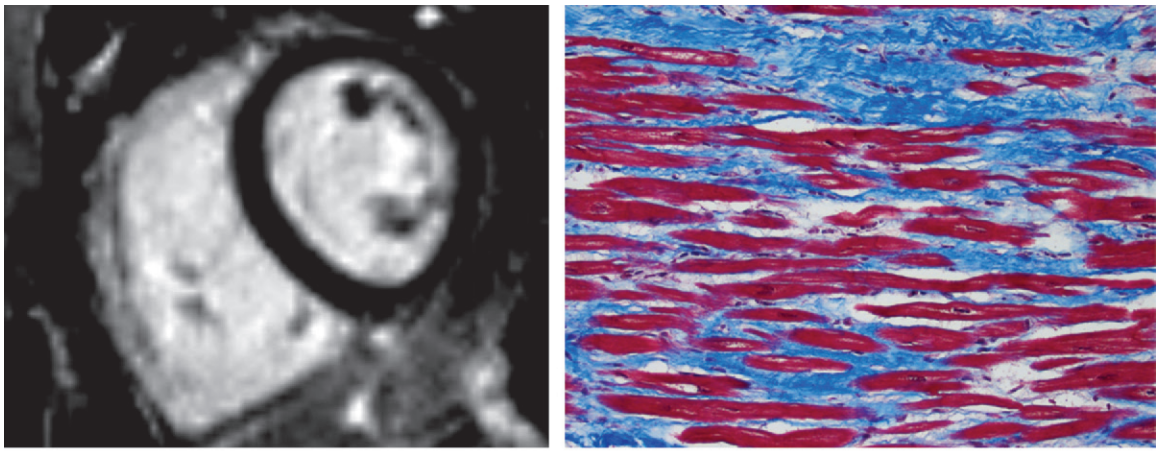

a. b.

Figure 4. Reactive interstitial fibrosis in a patient with arrhythmogenic right ventricular cardiomyopathy and dysplasia. **(a)** Short-axis delayed contrast-enhanced PSIR MR image obtained at 1.5 T shows an absence of late contrast enhancement. **(b)** Photomicrograph (Masson trichrome stain; original magnification, ×10) of endomyocardial biopsy specimen, obtained around the time that cardiac MR imaging was performed, shows moderate reactive interstitial fibrosis.

of inappropriate inversion time for nulling, and variations in signal enhancement—are also eliminated with this technique. As expected, precontrast enhancement T1 times in normal myocardium are much longer than postcontrast enhancement times, a result of the small amount of residual gadolinium in the myocardial interstitium, which has a relaxing effect (18). This relaxing effect is amplified by the increased volume of retained gadolinium in patients with diffuse fibrosis and even more so in patients with regional scarring. In animal and human studies, shortened T1 times in fibrotic myocardium on contrast-enhanced IR-prepared sequences showed good correlation with ex vivo fibrosis content (Fig 5) (39,43–46).

Teaching Point

T1 Mapping Techniques

How to Perform T1 Mapping

The T1 mapping sequence is acquired in a single breath hold. Multiple varieties of this basic IR-prepared sequence have been used, including the standard Look-Locker (LL) sequence, the modified LL inversion-recovery (MOLLI) sequence, and the shortened MOLLI (ShMOLLI) sequence. To measure T1 values, midventricular four-chamber long- and short-axis orientations are comparable (47). Some prefer to acquire three short-axis sections, including the base, midcavity, and apex to obtain a larger sample volume. Precontrast-enhanced T1 values may be used as a baseline reference and have been correlated with myocardial injury in patients with ischemic heart disease, hypertrophic cardiomyopathy, and dilated cardiomyopathy (40,48). Prolonged precontrast-enhanced T1 relaxation times are suggestive of diffuse fibrosis (compared with postcontrast-enhanced T1 relaxation times). Because gadolinium chelate is continuously excreted through the kidneys, T1 times of the myocardium vary during the washout phase (Fig 6) (49). To standardize this protocol, we acquire T1 times at 12 and 25 minutes after administering a consistent dose (0.15 mmol/kg) of gadolinium chelate, a protocol that is similar to that used in a large prospective clinical trial conducted at six centers in the United States and involving approximately 1200 study subjects (50,51).

Pulse sequences used to measure myocardial T1 times require electrocardiographic (ECG) gating to freeze cardiac motion, a unique requirement. In general, the most common approach uses an inversion recovery pulse sequence, in which application of a non–section-selective 180° pulse inverts the magnetization. As longitudinal magnetization recovers, at a time defined as the inversion time (TI), a section-selective 90° excitation pulse is applied and rotates the magnetization into the transverse plane. This "experiment" is repeated again and again, each time with the TI changed. To ensure complete T1 relaxation, the repetition time (TR) should be at least five times the T1 time (approximately 1000 msec for unenhanced myocardium). For cardiac applications, the TR is determined by the ECG R-R interval, which necessitates measuring the T1 time over multiple heartbeats.

To measure average myocardial T1 times, epicardial and endocardial contours are traced around the left ventricular myocardium. Alternatively, regions of interest may also be drawn

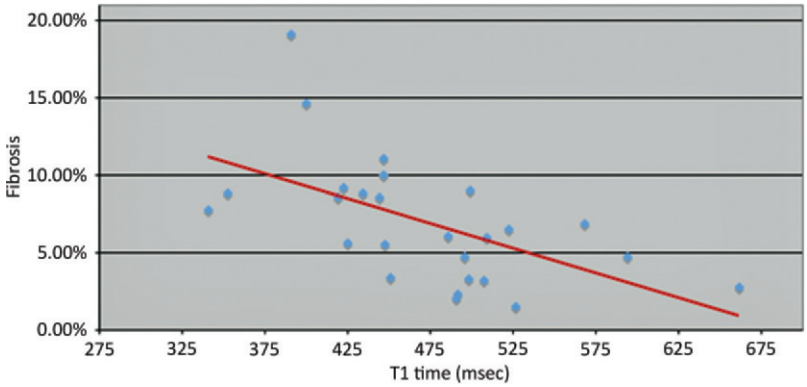

Figure 5. Graph plotting data from a study in which 26 patients underwent endomyocardial biopsy and cardiac MR imaging with an LL technique between January 2005 and January 2010 shows an inverse correlation between T1 time and percentage of patients with myocardial fibrosis (r =-0.57, $P < 0.0001$), which indicates that postcontrast T1 times reflect histologic findings. No late contrast enhancement (ie, regional scarring) was seen. Biopsy specimens underwent digitization and Masson trichrome staining by the pathology department at Johns Hopkins Hospital. With this method, the percentage of histologic fibrosis was correlated with corrected myocardial T1 times. (Reprinted and modified, with permission, from reference 46.)

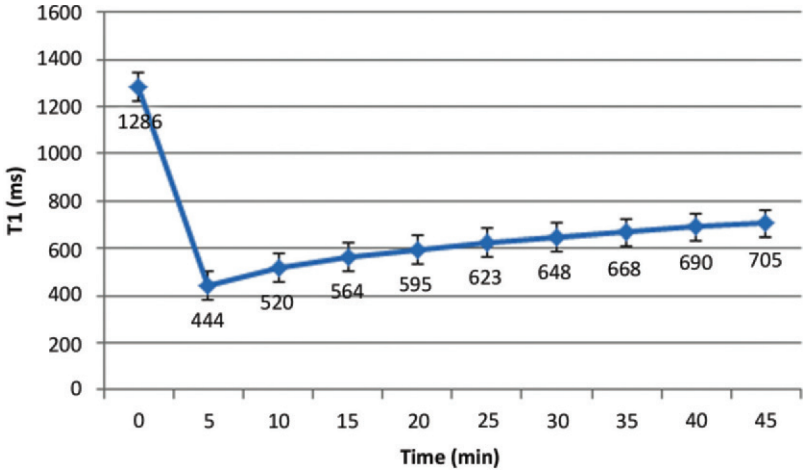

Figure 6. Graph shows myocardial T1 values that were obtained in a healthy volunteer at various times after intravenous administration of 0.15 mmol/kg gadopentetate dimeglumine. T1 values are expressed as the mean plus or minus the standard deviation.

for pooled blood or focal areas of myocardium. Postprocessing software, such as MASS V2010-EXP (Leidden University Medical Center, Leiden, The Netherlands), MRmap version 1.2 (Charite University Medicine, Berlin, Germany), and Vizpack (General Electric, Waukesha, Wis), may be used to derive the T1 relaxation time constant (Fig 7). Three-parameter curve fitting of data requires use of the Levenberg-Marquardt algorithm, which is calculated with one of the following equations: Mz (t) = A–Bexp (–R1*×t) and $Mz(t) = A–Be^{-R1*t}$, where Mz = sample magnetization at time, t = TI, and R1* = estimated relaxivity. A, B, and R1* are constants determined by curve-fitting the model to acquired phases. The equation T1 = (B/A–1) T1* is used to calculate the T1 time, where T1* is the modified T1 time in an LL experiment. Testing (χ^2) for fit excludes pixels with values that are not significant (level of significance: $\alpha = 0.05$). These steps are automatically performed by the analysis software (Fig 8).

In summary, the following basic steps are used for T1 mapping: ECG-gated contrast-enhanced IR-prepared LL sequences are performed, and the images are evaluated with postprocessing software such as MASS V2010-EXP. Endo- and epicardial contours or regions of interest are drawn to include the myocardial area of interest. T1 mapping software is used to perform three-parameter curve fitting of the data, and a T1 time is displayed. T1 times are compared with published values for normal healthy myocardium. In healthy myocardium, a contrast-enhanced T1 time that is lower than published T1 times is indicative of fibrosis.

Multiple approaches are currently available to derive an ECG-gated IR-prepared sequence, including the LL, MOLLI, and ShMOLLI techniques (Table 2) (52–55). Other less common sequences that may be used for T1 mapping include modulated repetition time LL, spin-and-stimulated-echo-planar imaging (two-dimensional [2D] ss-SESTEPI), variable sampling of k-space in time (VAST), and three-dimensional (3D) PSIR (39,56,57). An in-depth review of each of these sequences is beyond the scope of this discussion; however, LL, MOLLI, and ShMOLLI are further explored because of their relatively frequent appearances in recent publications.

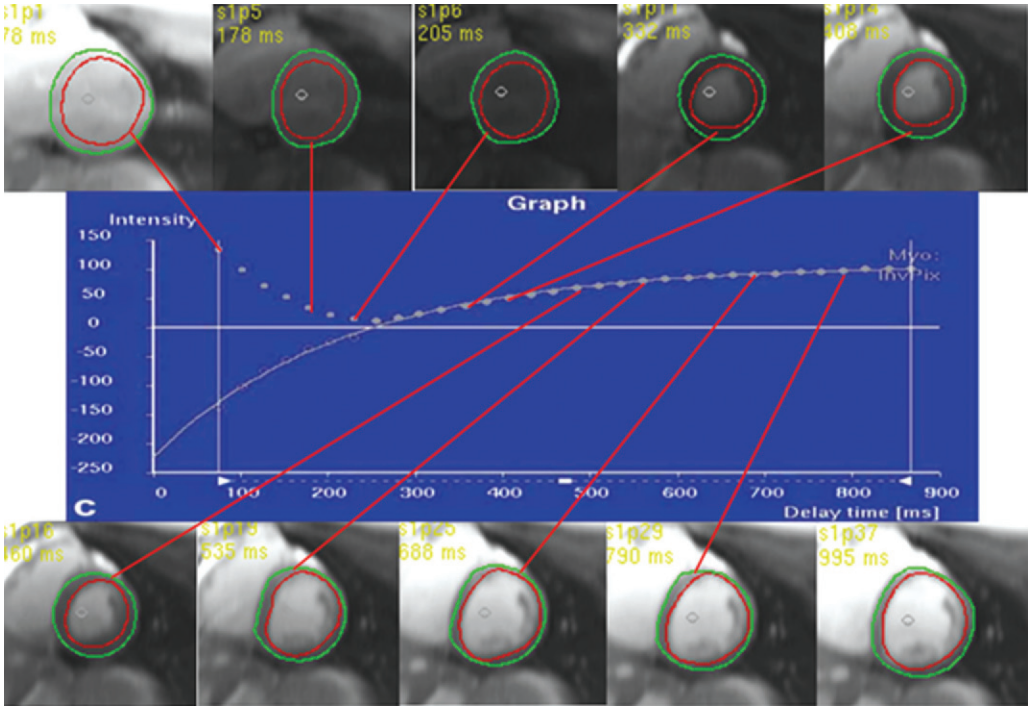

Figure 7. Graph shows curve fitting of selected short-axis sections from an LL sequence. Inversion times are shown in the upper left corner of each image.

Table 2: Typical Imaging Parameters of Common T1 Mapping Techniques

Parameter	LL	MOLLI	ShMOLLI
Field of view	360 × 290	360 × 250	340 × 255
Matrix size	192 × 72 to 192 × 93	192 × 122 to 192 × 183	192 × 144
Section thickness (mm)	8	8	8
Repetition time	2.5	2.2	2.1
Echo time	1.2	1.1	1.1
Flip angle	50	35	35
Parallel imaging factor	2	2	2
No. of images acquired	22–46*	11†	7‡
Acquisition window	35	191–202	206
Voxel size (mm)	1.7 × 2.7 × 8	1.6 × 2.3 × 8	0.9 × 0.9 × 8
Gadolinium dose (mmol/kg)	0.1–0.2	0.1–0.2	0.1–0.2

*The number of images acquired is determined by the heart rate.
†A set of three consecutive IR experiments with increasing TIs is performed throughout one breath hold, for a total of 11 images over 17 heartbeats.
‡A set of three consecutive IR experiments with increasing TIs are performed in one breath hold for a total of seven images acquired over nine heartbeats.

Look-Locker

The LL sequence is continuously and prospectively performed throughout the cardiac cycle, without regard for cardiac motion or gating to a specific phase (Fig 9). A single 180° pulse is applied, and images are acquired at multiple TIs. A variety of readout sequences have been used with the LL method, including steady-state free precession (SSFP), balanced SSFP, echoplanar imaging, and fast low-angle shot (FLASH), all of which enable LL images to be acquired in a single long breath hold (20–28 seconds). No matter which type of readout sequence is used, this sequence is referred to as a "TI scout" or LL sequence (Fig 10). The term *TI scout* refers to its use of multiple TIs to determine the null time of normal myocardium before delayed contrast-enhanced (scout) images are acquired. Because it is regularly performed before delayed contrast-enhanced images are acquired, the LL sequence is now ubiquitous in cardiac MR

Figure 8. T1 mapping performed with LL and MOLLI sequences in a 42-year-old man with mild asymmetric septal hypertrophy and mild to moderate systolic anterior motion of the mitral valve with provocation at echocardiography and a family history of hypertrophic cardiomyopathy. **(a–d)** Bright blood MR images obtained in the horizontal long-axis plane **(a)**, vertical long-axis plane **(b)**, five-chamber view **(c)**, and short-axis plane **(d)** show that mid septal thickness reaches 1.3 cm in end diastole. **(e–h)** Short-axis myocardial delayed enhancement MR images show an absence of late contrast enhancement *(continues)*.

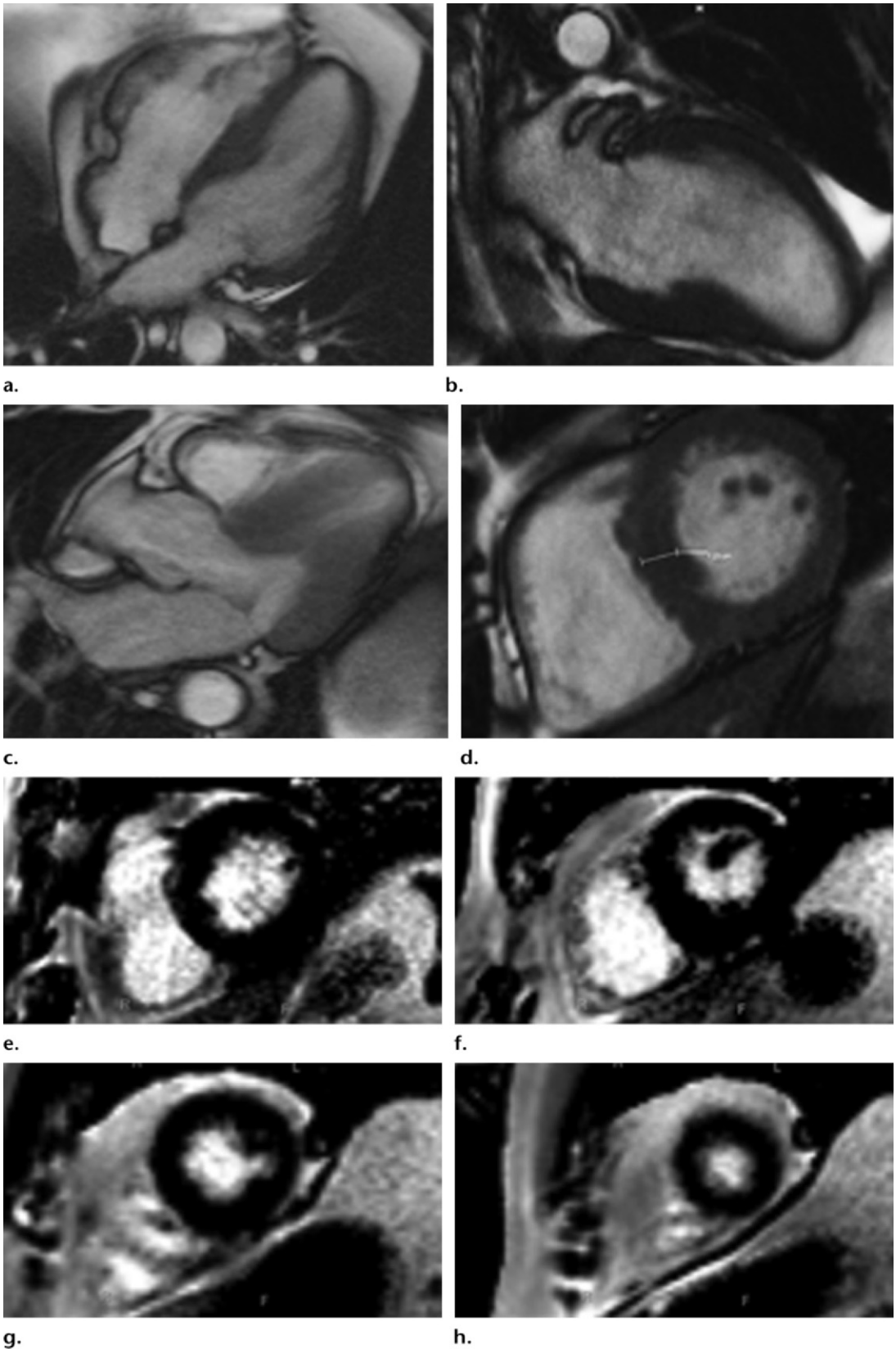

Figure 8. *(continued)* **(i, j)** Postcontrast T1 mapping performed with an LL sequence in the horizontal long-axis plane shows the left ventricular endo- (red line) and epicardial (green line) contours, which are manually drawn. Thirty-two images were acquired throughout the cardiac cycle. **(k)** Graph shows the data obtained from LL T1 mapping, which were plotted with three-parameter curve fitting and used to calculate T1 times. x-axis = delay time, y-axis = signal intensity. **(l, m)** Postcontrast T1 mapping performed with a MOLLI sequence in the short-axis plane shows the left ventricular endo- (red line) and epicardial (green line) contours, which are manually drawn. All 11 images were acquired at the same time in end diastole. **(n)** Graph shows the data obtained from MOLLI T1 mapping, which were plotted with three-parameter curve fitting and used to calculate T1 times. MOLLI and LL sequences had similar T1 values for T1 times after administration of gadolinium contrast material. x-axis = delay time, y-axis = signal intensity.

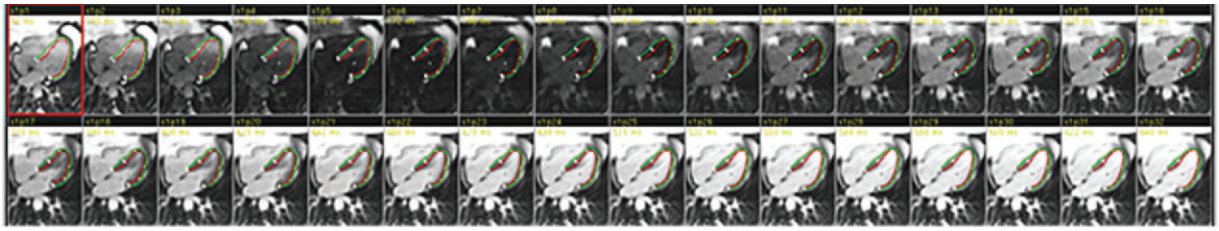

i.

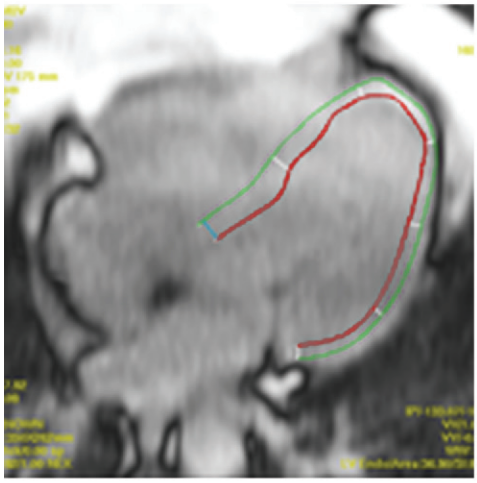

j.

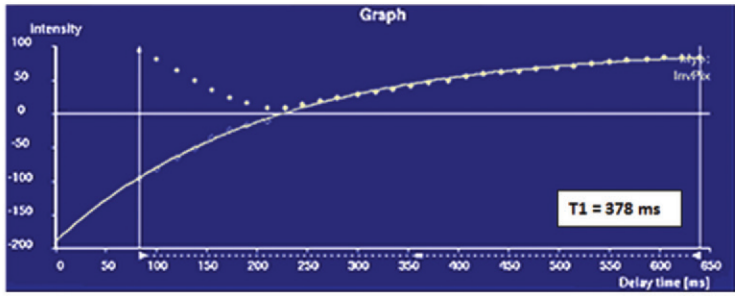

k.

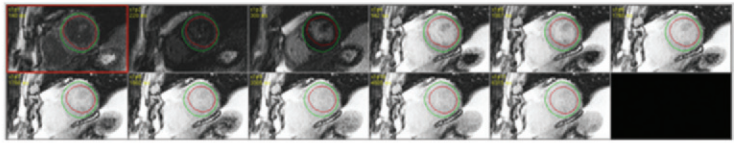

l.

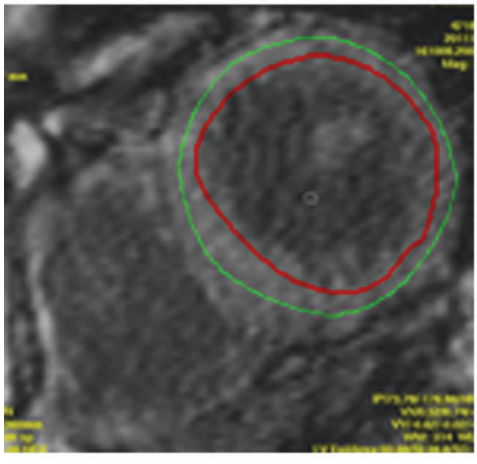

m.

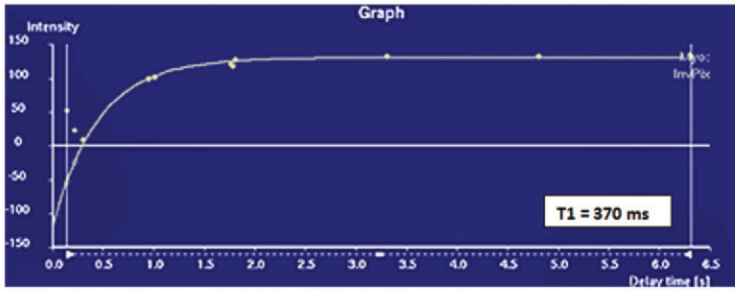

n.

imaging, leading to an abundance of retrospective data available for T1 mapping. Unfortunately, use of the LL sequence to perform pixel-by-pixel T1 mapping of the heart is limited by cardiac motion. Images are acquired throughout the cardiac cycle, with variations in image quality, depending on the heart rate and rhythm status. Regions of interest or endocardial and epicardial contours must be individually drawn on each image to determine a T1 time, a process that may be cumbersome and lead to inaccuracies due to misregistration.

MOLLI

To overcome the limitations of LL sequences, researchers developed a sequence that allows for selective data acquisition at a given time in the cardiac cycle (ie, end diastole) over successive heartbeats. A single image is acquired in each heartbeat, multiple images are acquired with each IR experiment, and a set of three consecutive IR experiments with increasing TIs

Figure 9. The first published myocardial T1 maps, which were obtained with the LL technique at 0.08 T in 1988, show that precontrast T1 values were higher in a patient with lupus erythematosus **(a)** than they were in the control patient **(b)**, a finding indicative of diffuse interstitial fibrosis. Each image in the T1 maps took about 5 minutes to acquire. (Reprinted, with permission, from reference 58.)

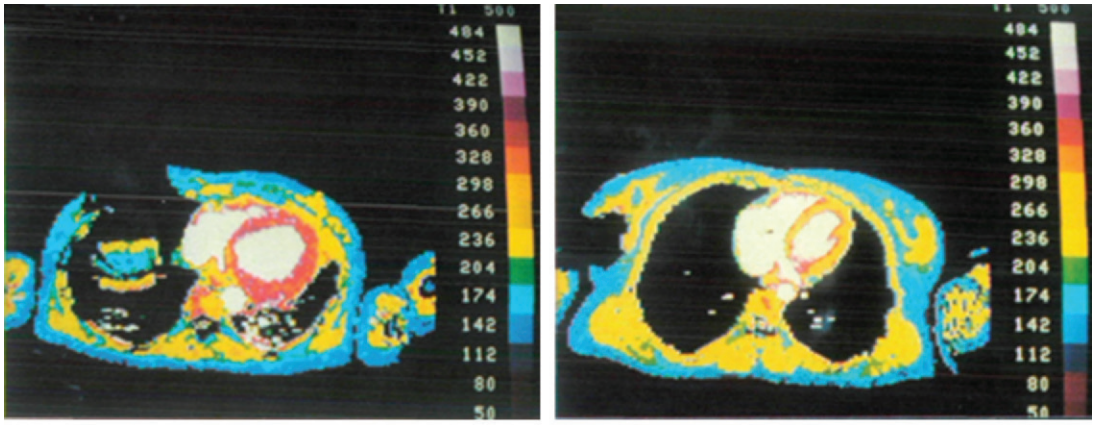

Figure 10. Diagram shows a conventional 2D LL pulse sequence, in which a nonselective 180° inversion pulse (π) is applied, and repeated radiofrequency pulses (α) with a small flip angle are separated by a time (τ) and sample the longitudinal signal magnetization as it recovers to steady state. μ = undisturbed recovery period. (Adapted and reprinted, with permission, from reference 45.)

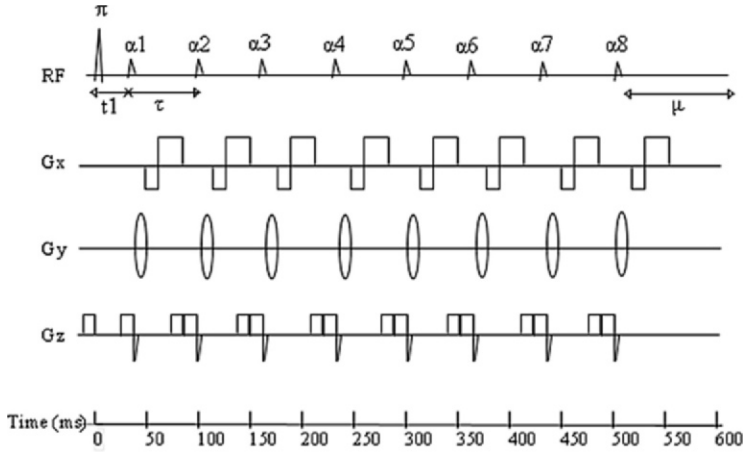

is performed throughout one breath hold, for a total of 11 images over 17 heartbeats. Cardiac motion is minimized by using a narrow acquisition window with parallel imaging techniques. Multiple studies have validated the accuracy of the use of MOLLI sequences for T1 mapping, with high levels of intra- and interobserver agreement (53,54,59). In a recent comparison of myocardial T1 mapping with LL and MOLLI by Nacif et al (47), both sequences had good agreement in intrasequence comparisons, but, in general, MOLLI had lower T1 values than LL and substantially tighter limits of agreement. The reported mean difference in T1 times between LL and MOLLI was +61.8 msec ± 46.4 ($P < .001$) (Fig 11).

Another advantage of MOLLI is its ability to merge the image sets from multiple IR acquisitions with varying TIs into a single data set. With some vendors, these data are automatically entered into three-parameter curve fitting at the scanner and T1 times are calculated. When used with inline motion correction, the T1 values for each voxel may be represented by signal intensity and displayed as a parametric color map image that may be displayed on workstations with standard picture archiving and communication (PACS) software, and T1 values may be directly derived by using regions of interest, negating the need for specialized T1 mapping software (Figs 12, 13) (60).

ShMOLLI

In an effort to decrease the relatively long breath hold (usually about 18 seconds) needed to perform the MOLLI sequence, Piechnik et al (55) investigated the use of a ShMOLLI sequence. On average, normal subjects could hold their breath for 20.9 seconds (range, 13–74 seconds) in end expiration (62). However, those with pulmonary disease could only hold their breath for an average of 9.1 seconds (range, 2–16 seconds) (62). Long breath holds are also a problem in patients with a low heart rate, resulting in breath holds longer than 20 seconds. With

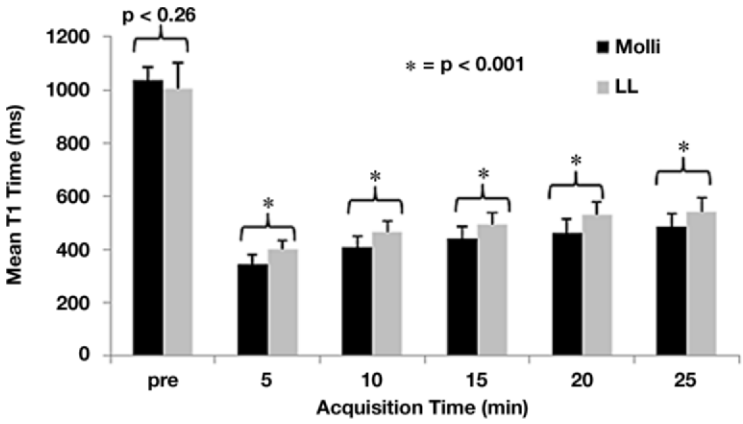

Figure 11. Graph shows the mean myocardial T1 time for each acquisition before and after (in 5-minute intervals) administration of contrast material with MOLLI (black) and LL (gray) sequences. For all postcontrast acquisitions, $P <$ .001; for precontrast acquisitions, $P = .26$. (Reprinted, with permission, from reference 47.)

Figure 12. T1 mapping in a patient with myocardial infarction. **(a)** Short-axis IR-prepared delayed contrast-enhanced MR image shows subendocardial enhancement in the anteroseptal wall and the subendocardial (red line), subepicardial (green line), and blood pool (yellow line) contours. **(b)** Short-axis color-scale parametric map, created with a 12-minute contrast-enhanced MOLLI sequence with inline motion correction, shows the T1 color scale, which indicates the T1 times of the left ventricular myocardium and blood pool. **(c)** Short-axis color-scale T1 parametric map shows the contours for infarction (white arrow), perinfarction (red arrow), and remote myocardium (black arrow), as well as the color scale with the corresponding T1 times. Contours were manually drawn on the basis of abnormal signal intensity on delayed contrast-enhanced images. (Images courtesy of Marcelo Nacif, MD, PhD, Universidade Federal Fluminense, Niterói, Brazil.)

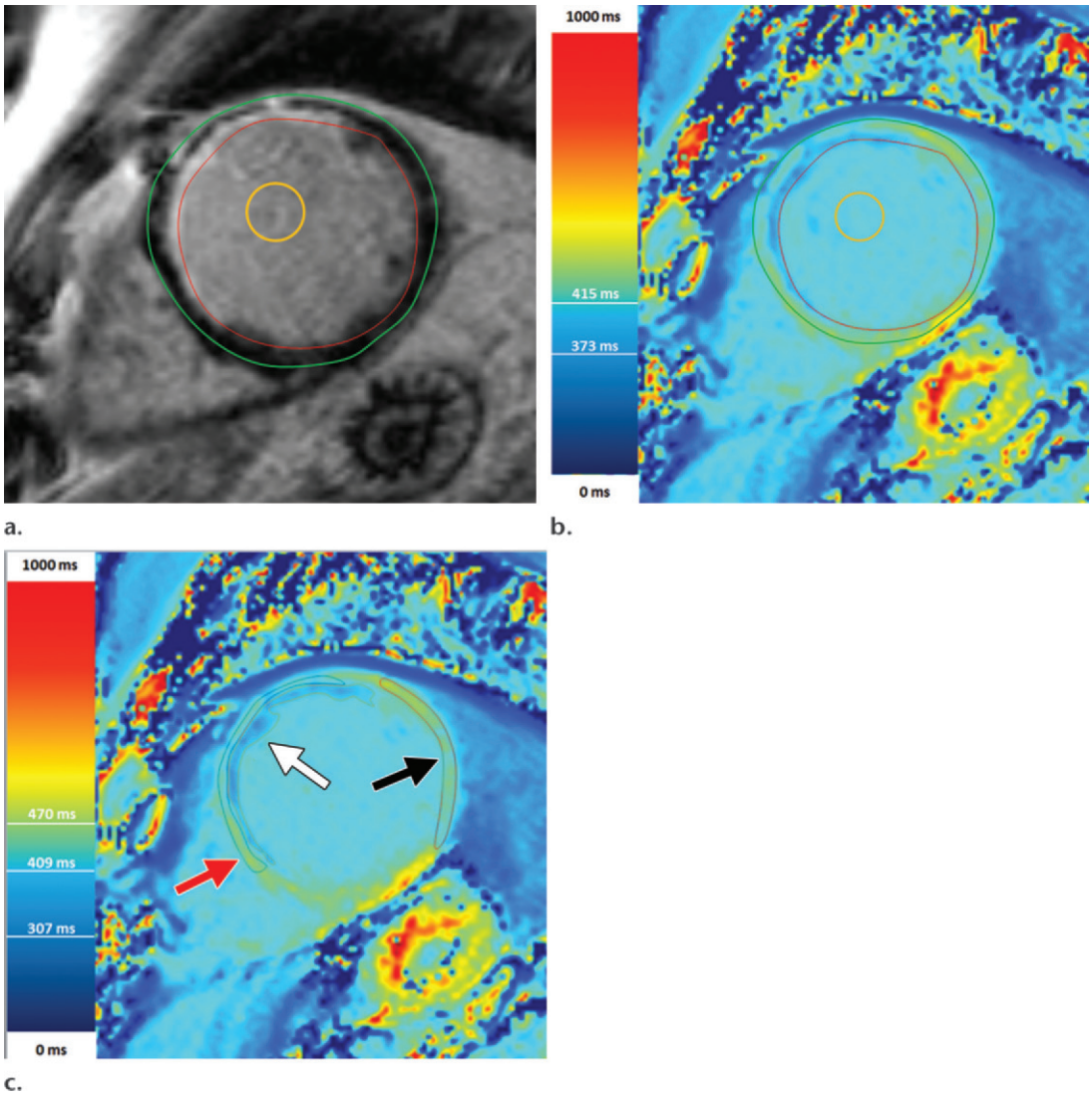

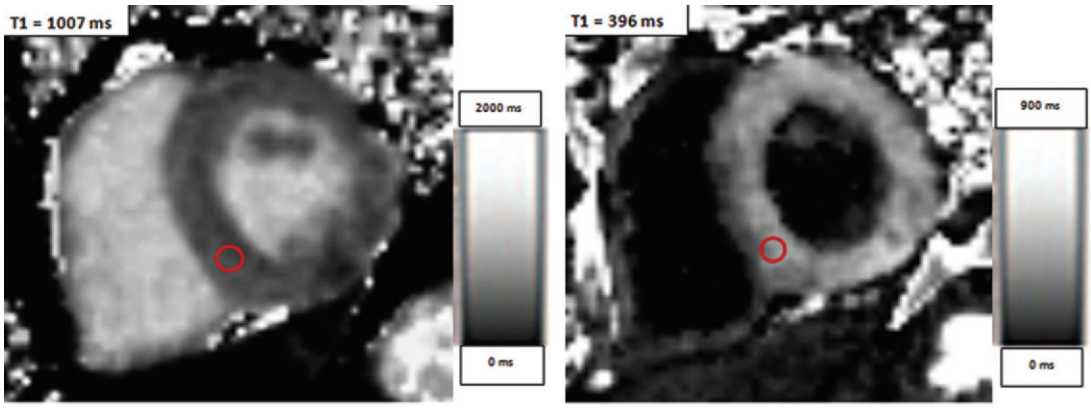

Figure 13. Use of regions of interest to derive T1 values in a patient with hypertrophic cardiomyopathy. Short-axis gray-scale parametric T1 maps obtained with MOLLI sequences and inline motion correction before **(a)** and 12 minutes after **(b)** administration of contrast material show the regions of interest (circle) and T1 times. Typically, postcontrast T1 times are 450–475 msec. In this case, the T1 time was 396 msec, a finding indicative of diffuse myocardial fibrosis, which, when associated with hypertrophic cardiomyopathy, may be seen at cardiac MR imaging and is associated with left ventricular diastolic dysfunction.

the ShMOLLI sequence, the average breath hold decreases to 9.1 seconds (±1.1 seconds), and the number of required heartbeats decreases from 17 to nine. In the study by Piechnik et al (55), T1 times less than 1200 msec obtained with a ShMOLLI sequence had good agreement with those obtained with MOLLI sequences (Fig 14).

Extracellular Volume Fraction

An essential component of quantitative imaging is the ability to compare calculated T1 times with standardized control values to determine the presence and extent of disease. Comparing T1 times in different patients has been complicated by differences in patient-specific factors, such as heart rate, gadolinium dose, timing of image acquisition after administration of intravenous contrast material, hematocrit level, body composition, B_0 field, and glomerular filtration rate, which may cause small but important changes in measured T1 times. For example, Gai et al (63) reported that precontrast T1 times have a strong linear dependence on heart rate; however, there was no significant relationship between heart rate and postcontrast T1 times. Investigators developed mathematic models by using correction values for the most important of these variables, including heart rate. Corrected T1 values obtained in a population of patients with type I diabetes were more tightly clustered and showed better discrimination of patients with disease from healthy control subjects (63). However, thus far, histologic validation of these complex models has been limited to animals and ex vivo tissue samples, and these models account for only some of the patient-specific factors (43,44).

Recent research on T1 mapping focuses on the use of extracellular volume fraction (ECV) to quantify myocardial fibrosis (64–69). Compared with standard T1 mapping techniques, ECV is not affected by many of the previously described patient-specific factors and allows for more accurate patient-to-patient comparisons (66,67). Investigators have shown that myocardial gadolinium distribution volume correlates with histologic collagen volume fraction in vitro and in vivo (66,67). In the two-compartment model, a dynamic equilibrium between plasma and myocardial interstitium occurs approximately 8.5 minutes after administration of a bolus of gadolinium chelate and remains at a steady state up to 50 minutes after administration of contrast material (64). Myocardium that contains diffuse or regional fibrosis could delay the time to reach steady-state equilibrium. ECV is calculated by measuring the myocardial gadolinium distribution volume, which is determined by the patient's hematocrit level to adjust the gadolinium contrast partition coefficient. In one technique, quantitative parametric images of myocardial ECV are acquired with MOLLI sequences performed before and after intravenous administration of gadolinium-based extracellular contrast material (69). Because the time to achieve equilibrium of gadolinium between the myocardial and blood pools is delayed in patients with diseased or infarcted myocardium, we generally obtain ECV measurements 0, 12, and 25 minutes after administration of gadolinium. Data obtained from these T1 maps are used with the hematocrit level to calculate ECV, which ranges from 0% to 100%, with normal values between 20% and 32% (mean, plus or minus two standard deviations) (Fig 15).

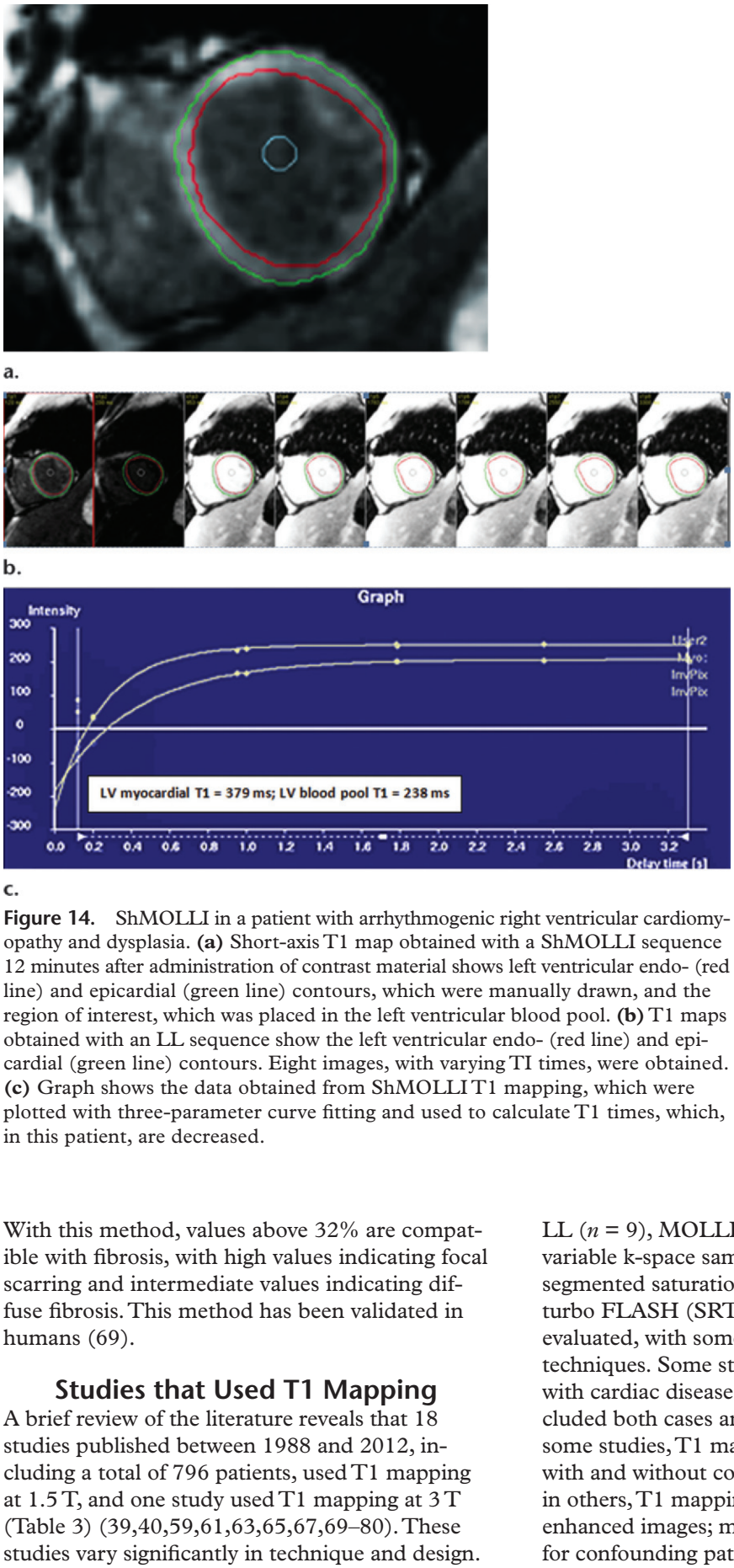

Figure 14. ShMOLLI in a patient with arrhythmogenic right ventricular cardiomyopathy and dysplasia. **(a)** Short-axis T1 map obtained with a ShMOLLI sequence 12 minutes after administration of contrast material shows left ventricular endo- (red line) and epicardial (green line) contours, which were manually drawn, and the region of interest, which was placed in the left ventricular blood pool. **(b)** T1 maps obtained with an LL sequence show the left ventricular endo- (red line) and epicardial (green line) contours. Eight images, with varying TI times, were obtained. **(c)** Graph shows the data obtained from ShMOLLI T1 mapping, which were plotted with three-parameter curve fitting and used to calculate T1 times, which, in this patient, are decreased.

With this method, values above 32% are compatible with fibrosis, with high values indicating focal scarring and intermediate values indicating diffuse fibrosis. This method has been validated in humans (69).

Studies that Used T1 Mapping

A brief review of the literature reveals that 18 studies published between 1988 and 2012, including a total of 796 patients, used T1 mapping at 1.5 T, and one study used T1 mapping at 3 T (Table 3) (39,40,59,61,63,65,67,69–80). These studies vary significantly in technique and design. LL (n = 9), MOLLI (n = 6), ShMOLLI (n = 1), variable k-space sampling (VAST; n = 2), and segmented saturation-recovery single breath-hold turbo FLASH (SRTFL; n = 1) techniques were evaluated, with some studies evaluating multiple techniques. Some studies only included patients with cardiac disease (n = 4). Most studies included both cases and controls (n = 15), and in some studies, T1 mapping was performed both with and without contrast enhancement, whereas in others, T1 mapping was only performed on unenhanced images; most studies did not normalize for confounding patient-specific factors.

Table 3: Cardiovascular Diseases Previously Evaluated with T1 Mapping

Author and Date (Reference no.)	Cardiac Disease	Technique	Sample Size (Cases/Controls)	Pre-/Postcontrast T1 values (msec)		Conclusions
				Case	Control	
Messroghli 2003 (68)	Acute myocardial infarction	LL	8/8	849 ± 60/262 ± 19	721 ± 37/362 ± 27*	Postcontrast myocardial T1 values in acute myocardial infarction were significantly reduced compared with remote myocardium
Klein 2004 (69)	Ischemic cardiomyopathy	MOLLI	11/2	720 ± 18/250 ± 30	720 ± 11/340 ± 40	In ischemic cardiomyopathy, postcontrast T1 values were significantly reduced compared with normal myocardium
Maceira 2005 (70)	Amyloidosis	LL	22/16	NR/427 ± 73	NR/579 ± 75	Subepicardial postcontrast T1 values were significantly reduced in amyloid compared with controls
Sparrow 2006 (71)	Chronic aortic regurgitation	MOLLI	8/15	1000/580	980/570†	No significant difference in pre- and postcontrast myocardial T1 values compared with healthy controls; subgroup analysis showed significantly reduced postcontrast T1 values in segments with abnormal wall motion
Messroghli 2007 (57)	Acute or chronic myocardial infarction	MOLLI	24/24	Acute: 1197 ± 76/NR; chronic: 1060 ± 61/NR	Acute: 1011 ± 66/494 ± 23*; chronic: 987 ± 34/NR*	In acute and chronic infarction, precontrast T1 values were higher than T1 values in remote myocardium
Hosch 2007 (72)	Amyloidosis	SRTFL	19/10	1340 ± 81/NR	1146 ± 71/NR	Precontrast myocardial T1 values were higher in amyloidosis than in healthy controls
Iles 2008 (39)	Chronic heart failure	VAST	25/20	NR/429 ± 22	NR/564 ± 23	Postcontrast myocardial T1 values in chronic heart failure were significantly reduced compared with controls; reduced T1 times appear to reflect diffuse fibrosis when histologically correlated with biopsy samples
Maceira 2008 (73)	Amyloidosis	LL	29/0	NR	NR	Differences in postcontrast T1 values in subepicardium and subendocardium indicated mortality in cardiac amyloidosis
Amano 2009 (74)	HCM	LL	23/7	NR	NR	Null points at contrast-enhanced LL were significantly shorter than for blood, normal myocardium, and nullified myocardium of HCM

Note.—DCM = dilated cardiomyopathy, HCM = hypertrophic cardiomyopathy, NICM = nonischemic cardiomyopathy, NR = not reported, SRTFL = saturation-recovery turbo FLASH. All sequences were performed on a 1.5-T imager unless otherwise specified. *Remote myocardium was used as the control. †The standard deviation was not published. ‡According to the fibrosis index. §A 3-T imager was used.

(continues)

Table 3: Cardiovascular Diseases Previously Evaluated with T1 Mapping *(continued)*

Author and Date (Reference no.)	Cardiac Disease	Technique	Sample Size (Cases/ Controls)	Pre-/Postcontrast T1 values (msec)		Conclusions
				Case	Control	
Broberg 2010 (63)	Adult congenital heart disease	LL	50/14	31.9 ± 4.9%‡	24.8 ± 2.0%‡	Fibrosis index is elevated in patients with adult congenital heart disease
Flett 2010 (65)	Aortic stenosis, HCM	LL	18/8 (aortic stenosis), 8/8 (HCM)	NR	NR	T1 mapping with equilibrium contrast cardiac MR imaging had a high correlation with histologic samples of aortic stenosis and HCM
Gai 2011 (61)	Type 1 diabetes	LL	19/13	NR/548 ± 59 (low risk), NR/499 ± 59 (high risk)	983 ± 84/537 ± 22	After adjusting for factors that affect patient comparisons, there was a significant difference in postcontrast T1 values in those at low risk for diabetes compared with those at high risk
Jellis 2011 (75)	Type 2 diabetes	MOLLI	67/0	830 ± 168/434 ± 64	NR	Diffuse myocardial fibrosis is an underlying contributor to early diabetic cardiomyopathy; reduced postcontrast T1 values are associated with diastolic dysfunction in diabetes
Ng 2011 (76)	Types 1 and 2 diabetes	LL	50/19	NR/425 ± 72	NR/504 ± 34	Reduced T1 values are associated with impaired systolic and diastolic function in diabetes
Ugander 2012 (67)	NICM; prior myocardial infarction	MOLLI	30/11; 36/11	ECV = 37 ± 6% (NICM), ECV = 51 ± 8% (myocardial infarction)	ECV = 26 ± 3% (NICM), ECV = 26 ± 3% (myocardial infarction)	Myocardial ECV is elevated in those with NICM and prior myocardial infarction
Bauner 2012 (77)	Chronic myocardial infarction	MOLLI	26/26	1160 ± 80/239 ± 74; ECV = 54% ± 10%	1001 ± 47/380 ± 59; ECV = 28%±5%	Postcontrast T1 values in chronically infarcted myocardium are significantly different from those in healthy myocardium
Turkbey 2012 (78)	Myotonic muscular dystrophy	LL	33/13	NR/394 ± 58	NR/441 ± 32	Postcontrast T1 values were lower in myotonic muscular dystrophy than in controls, likely due to diffuse myocardial fibrosis
Ellims 2012 (59)	HCM	VAST	51/25	NR/483 ± 85	NR/561 ± 47	Subjects with HCM had lower postcontrast myocardial T1 values than did controls
Dass 2012 (40)	HCM, DCM§	ShMOLLI	28/12 (HCM), 18/12 (DCM)	1228 ± 32 (HCM), 1228 ± 36/NR (DCM)	1190 ± 20/NR	Those with HCM or DCM had higher precontrast myocardial T1 values than did controls

Note.—DCM = dilated cardiomyopathy, HCM = hypertrophic cardiomyopathy, NICM = nonischemic cardiomyopathy, NR = not reported, SRTFL = saturation-recovery turbo FLASH. All sequences were performed on a 1.5-T imager unless otherwise specified. *Remote myocardium was used as the control. †The standard deviation was not published. ‡According to the fibrosis index. §A 3-T imager was used.

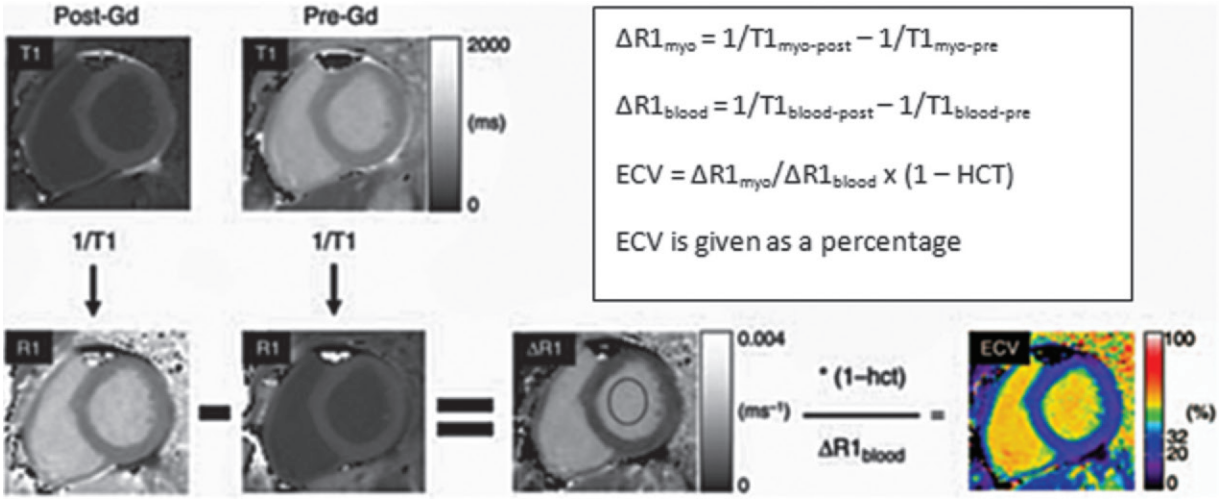

Figure 15. Chart shows the calculation of ECV, in which a reciprocal of the signal in each pixel (1/T1) is used to generate an R1 map. The precontrast R1 map is subtracted from the postcontrast R1 map to generate a ΔR1 map. A ΔR1 map of the blood pool ($\Delta R1_{blood}$) is measured by placing a region of interest in the left ventricular blood pool. To calculate ECV, ΔR1 map pixel values are multiplied by one, with the hematocrit level subtracted, and then divided by the mean $\Delta R1_{blood}$. The final result is a parametric map that displays the pixel-by-pixel ECV values, which are converted into signal intensity by the software. (Adapted and reprinted, with permission, from reference 69.)

Teaching Point

Despite the diversity of these studies, a clear pattern is manifest: In general, postcontrast myocardial T1 relaxation times are shorter in patients with cardiac disease than they are in healthy control subjects. Unfortunately, a direct comparison of T1 times between studies is limited because of variations in imaging technique and methods of analysis. In control subjects, normal postcontrast myocardial T1 times are reported to be 340–579 msec, whereas those in patients with cardiac disease are reported to be 250–580 msec (Table 3). In control subjects, the differences in T1 values with the LL and MOLLI techniques correspond well with the comparison performed by Nacif et al (47).

Multiple studies have also examined the use of ECV and cardiovascular diseases such as acute myocarditis, chronic myocardial infarction, hypertrophic cardiomyopathy, nonischemic dilated cardiomyopathy, cardiac amyloidosis, and systemic capillary leak syndrome. One of the larger studies by Kellman et al (81) reported an ECV of 25.4 ± 2.5% (mean plus or minus the standard deviation) in 62 healthy patients, with a range of 20%–30%. Among those with cardiac disease, ECV was 32%–69%.

To our knowledge, three studies on the diagnostic accuracy of myocardial T1 mapping have been published to date. In a study that included 26 patients, Bauner et al (79) reported that contrast-enhanced T1 mapping with a T1 threshold of 305 msec or less had sensitivity and specificity of 96% and 99%, respectively, for depicting chronic myocardial infarction. In the same group of patients, ECV had sensitivity and specificity of 96% and 100%, respectively, with a threshold over 42%.

Ferreira et al (82) reported that, in 21 patients with acute regional myocardial edema and no infarction and 21 healthy patients, unenhanced T1 mapping with a threshold of 990 msec had sensitivity and specificity of 92%. Messroghli et al (59) evaluated 24 patients with acute infarction, compared their findings with previously published findings in healthy volunteers, and reported that precontrast T1 mapping with a threshold of 1120 msec or more (mean plus three standard deviations) had sensitivity and specificity of 96% and 91%, respectively. Postcontrast T1 mapping with a threshold of 392 msec or less (mean plus three standard deviations) was reported to have sensitivity and specificity of 100% and 95%, respectively, in patients with chronic myocardial infarction.

Potential Future Applications of Cardiac T1 Mapping

There are many questions about T1 mapping that remain unanswered, such as the optimal technique for performing IR experiments, whether T1 normalization is necessary, the optimal placement of the region of interest, and whether to correlate T1 shortening with disease progression or outcomes. Myocardial T1 mapping may have applications in many cardiac diseases in which diffuse interstitial fibrosis develops that have not yet been researched, such as primary cardiac diseases (eg, arrhythmogenic right ventricular cardiomyopathy and dysplasia and myocarditis), mitral and tricuspid valvular disease, arrhythmogenic cardiac diseases (eg, atrial

fibrillation, atrial flutter, and idiopathic right ventricular outflow tract ventricular tachycardia), systemic disorders that affect the heart (eg, collagen vascular diseases, toxic cardiomyopathies, systemic hypertension, chronic renal disease, and sarcoidosis), and pulmonary artery hypertension. Myocardial T1 mapping also has the potential to depict early rejection of transplanted hearts, which may obviate the need for more invasive endomyocardial biopsy. Given the central importance of myocardial fibrosis as a common and final pathway in an array of cardiac diseases, myocardial T1 mapping has the potential to play an important role in establishing a diagnosis and prognosis and providing a therapeutic assessment in patients with cardiac disease, and it appears that our current research has revealed only the tip of a very large iceberg.

Summary

In the heart, diffuse interstitial fibrosis plays an essential role in the development of a variety of cardiomyopathies and is associated with increased mortality. Previously, endomyocardial biopsy was the principle method used to diagnose myocardial fibrosis. Currently, late contrast-enhanced cardiac MR imaging is a robust, well-validated, noninvasive method for identifying replacement fibrosis (ie, scarring). T1 mapping of diffuse interstitial fibrosis of the myocardium is a novel and expanding application of cardiac MR imaging and has the potential to depict diffuse interstitial fibrosis in a variety of cardiac diseases. Standardization of myocardial T1 mapping techniques will help determine potential cutoff values for identifying normal and diseased myocardium in future clinical trials.

References

1. Kwong RY, Chan AK, Brown KA, et al. Impact of unrecognized myocardial scar detected by cardiac magnetic resonance imaging on event-free survival in patients presenting with signs or symptoms of coronary artery disease. Circulation 2006;113(23):2733–2743.
2. Kwong RY, Sattar H, Wu H, et al. Incidence and prognostic implication of unrecognized myocardial scar characterized by cardiac magnetic resonance in diabetic patients without clinical evidence of myocardial infarction. Circulation 2008;118(10):1011–1020.
3. Assomull RG, Prasad SK, Lyne J, et al. Cardiovascular magnetic resonance, fibrosis, and prognosis in dilated cardiomyopathy. J Am Coll Cardiol 2006;48(10):1977–1985.
4. Dweck MR, Joshi S, Murigu T, et al. Midwall fibrosis is an independent predictor of mortality in patients with aortic stenosis. J Am Coll Cardiol 2011;58(12):1271–1279.
5. Becker AE, Heijmans CD, Essed CE. Chronic non-ischaemic congestive heart disease and endomyocardial biopsies: worth the extra? Eur Heart J 1991;12(2):218–223.
6. Libby P, Lee RT. Matrix matters. Circulation 2000;102(16):1874–1876.
7. Speiser B, Riess CF, Schaper J. The extracellular matrix in human myocardium. I. Collagens I, III, IV, and VI. Cardioscience 1991;2(4):225–232.
8. Speiser B, Weihrauch D, Riess CF, Schaper J. The extracellular matrix in human cardiac tissue. II. Vimentin, laminin, and fibronectin. Cardioscience 1992;3(1):41–49.
9. Rossi MA. Connective tissue skeleton in the normal left ventricle and in hypertensive left ventricular hypertrophy and chronic chagasic myocarditis. Med Sci Monit 2001;7(4):820–832.
10. Caspari PG, Gibson K, Harris P. Changes in myocardial collagen in normal development and after beta-blockade. In: Harris P, Bing RJ, Fleckenstein A, eds. Biochemistry and pharmacology of myocardial hypertrophy, hypoxia, and infarction. Baltimore, Md: University Park Press, 1976; 99–104.
11. Bujak M, Frangogiannis NG. The role of TGF-beta signaling in myocardial infarction and cardiac remodeling. Cardiovasc Res 2007;74(2):184–195.
12. Swynghedauw B. Molecular mechanisms of myocardial remodeling. Physiol Rev 1999;79(1):215–262.
13. Wynn TA. Cellular and molecular mechanisms of fibrosis. J Pathol 2008;214(2):199–210.
14. Anderson KR, Sutton MG, Lie JT. Histopathological types of cardiac fibrosis in myocardial disease. J Pathol 1979;128(2):79–85.
15. Sutton MG, Sharpe N. Left ventricular remodeling after myocardial infarction: pathophysiology and therapy. Circulation 2000;101(25):2981–2988.
16. Bohl S, Wassmuth R, Abdel-Aty H, et al. Delayed enhancement cardiac magnetic resonance imaging reveals typical patterns of myocardial injury in patients with various forms of non-ischemic heart disease. Int J Cardiovasc Imaging 2008;24(6):597–607.
17. Karamitsos TD, Francis JM, Myerson S, Selvanayagam JB, Neubauer S. The role of cardiovascular magnetic resonance imaging in heart failure. J Am Coll Cardiol 2009;54(15):1407–1424.
18. Vogel-Claussen J, Rochitte CE, Wu KC, et al. Delayed enhancement MR imaging: utility in myocardial assessment. RadioGraphics 2006;26(3):795–810.
19. Sangaralingham SJ, Huntley BK, Martin FL, et al. The aging heart, myocardial fibrosis, and its relationship to circulating C-type natriuretic peptide. Hypertension 2011;57(2):201–207.
20. Spector KS. Diabetic cardiomyopathy. Clin Cardiol 1998;21(12):885–887.
21. Gramley F, Lorenzen J, Pezzella F, et al. Hypoxia and myocardial remodeling in human cardiac allografts: a time-course study. J Heart Lung Transplant 2009;28(11):1119–1126.
22. Corrado D, Basso C, Thiene G, et al. Spectrum of clinicopathologic manifestations of arrhythmogenic right ventricular cardiomyopathy/dysplasia: a multicenter study. J Am Coll Cardiol 1997;30(6):1512–1520.
23. Strauss DG, Selvester RH, Dibernardo LR. Myocardial scar in sarcoidosis by 12-lead ECG and pathology. Ann Noninvasive Electrocardiol 2011;16(2):219–222.
24. Brigden W, Bywaters EGL, Lessof MH, Ross IP. The heart in systemic lupus erythematosus. Br Heart J 1960;22:1–16.
25. Allanore Y, Meune C. Primary myocardial involvement in systemic sclerosis: evidence for a microvascular origin. Clin Exp Rheumatol 2010;28(5, suppl 62):S48–S53.

26. Losi MA, Memoli B, Contaldi C, et al. Myocardial fibrosis and diastolic dysfunction in patients on chronic haemodialysis. Nephrol Dial Transplant 2010;25(6):1950–1954.
27. Hosch W, Kristen AV, Libicher M, et al. Late enhancement in cardiac amyloidosis: correlation of MRI enhancement pattern with histopathological findings. Amyloid 2008;15(3):196–204.
28. Moon JC, Sachdev B, Elkington AG, et al. Gadolinium enhanced cardiovascular magnetic resonance in Anderson-Fabry disease: evidence for a disease specific abnormality of the myocardial interstitium. Eur Heart J 2003;24(23):2151–2155.
29. Babu-Narayan SV, McCarthy KP, Ho SY, Magee AG, Kilner PJ, Sheppard MN. Images in cardiovascular medicine: myocarditis and sudden cardiac death in the young—extensive fibrosis suggested by cardiovascular magnetic resonance in vivo and confirmed post mortem. Circulation 2007;116(6): e122–e125.
30. Dettmeyer R, Friedrich K, Schmidt P, Madea B. Heroin-associated myocardial damages: conventional and immunohistochemical investigations. Forensic Sci Int 2009;187(1-3):42–46.
31. Weber KT, Brilla CG. Pathological hypertrophy and cardiac interstitium: fibrosis and renin-angiotensin-aldosterone system. Circulation 1991;83(6): 1849–1865.
32. Weber KT, Janicki JS, Shroff SG, Pick R, Chen RM, Bashey RI. Collagen remodeling of the pressure-overloaded, hypertrophied nonhuman primate myocardium. Circ Res 1988;62(4):757–765.
33. Schaper J, Speiser B. The extracellular matrix in the failing human heart. Basic Res Cardiol 1992;87 (suppl 1):303–309.
34. O'Hanlon R, Grasso A, Roughton M, et al. Prognostic significance of myocardial fibrosis in hypertrophic cardiomyopathy. J Am Coll Cardiol 2010; 56(11):867–874.
35. Villari B, Campbell SE, Hess OM, et al. Influence of collagen network on left ventricular systolic and diastolic function in aortic valve disease. J Am Coll Cardiol 1993;22(5):1477–1484.
36. Pitt B, Zannad F, Remme WJ, et al. The effect of spironolactone on morbidity and mortality in patients with severe heart failure: randomized aldactone evaluation study investigators. N Engl J Med 1999;341(10):709–717.
37. Zannad F, Alla F, Dousset B, Perez A, Pitt B. Limitation of excessive extracellular matrix turnover may contribute to survival benefit of spironolactone therapy in patients with congestive heart failure: insights from the randomized aldactone evaluation study (RALES). RALES Investigators. Circulation 2000;102(22):2700–2706.
38. Rodgers CT, Robson MD. Cardiovascular magnetic resonance: physics and terminology. Prog Cardiovasc Dis 2011;54(3):181–190.
39. Iles L, Pfluger H, Phrommintikul A, et al. Evaluation of diffuse myocardial fibrosis in heart failure with cardiac magnetic resonance contrast-enhanced T1 mapping. J Am Coll Cardiol 2008;52 (19):1574–1580.
40. Dass S, Suttie JJ, Piechnik SK, et al. Myocardial tissue characterization using magnetic resonance noncontrast T1 mapping in hypertrophic and dilated cardiomyopathy. Circ Cardiovasc Imaging 2012;5 (6):726–733.
41. Kim RJ, Chen EL, Lima JA, Judd RM. Myocardial Gd-DTPA kinetics determine MRI contrast enhancement and reflect the extent and severity of myocardial injury after acute reperfused infarction. Circulation 1996;94(12):3318–3326.
42. Scholz TD, Fleagle SR, Burns TL, Skorton DJ. Nuclear magnetic resonance relaxometry of the normal heart: relationship between collagen content and relaxation times of the four chambers. Magn Reson Imaging 1989;7(6):643–648.
43. Grover-McKay M, Scholz TD, Burns TL, Skorton DJ. Myocardial collagen concentration and nuclear magnetic resonance relaxation times in the spontaneously hypertensive rat. Invest Radiol 1991;26 (3):227–232.
44. Messroghli DR, Nordmeyer S, Dietrich T, et al. Assessment of diffuse myocardial fibrosis in rats using small-animal Look-Locker inversion recovery T1 mapping. Circ Cardiovasc Imaging 2011;4(6): 636–640.
45. Henderson E, McKinnon G, Lee TY, Rutt BK. A fast 3D Look-Locker method for volumetric T1 mapping. Magn Reson Imaging 1999;17(8):1163–1171.
46. Sibley CT, Noureldin RA, Gai N, et al. T1 Mapping in cardiomyopathy at cardiac MR: comparison with endomyocardial biopsy. Radiology 2012;265 (3):724–732.
47. Nacif MS, Turkbey EB, Gai N, et al. Myocardial T1 mapping with MRI: comparison of Look-Locker and MOLLI sequences. J Magn Reson Imaging 2011;34 (6):1367–1373.
48. Dall'Armellina E, Piechnik SK, Ferreira VM, et al. Cardiovascular magnetic resonance by noncontrast T1-mapping allows assessment of severity of injury in acute myocardial infarction. J Cardiovasc Magn Reson 2012;14(1):article 15.
49. Judd RM, Kim RJ. Imaging time after Gd-DTPA injection is critical in using delayed enhancement to determine infarct size accurately with magnetic resonance imaging. Circulation 2002;106(2):e6; author reply e6.
50. Bild DE, Bluemke DA, Burke GL, et al. Multi-ethnic study of atherosclerosis: objectives and design. Am J Epidemiol 2002;156(9):871–881.
51. Liu CY, Liu YC, Wu C, et al. Evaluation of age-related interstitial myocardial fibrosis with cardiac magnetic resonance contrast-enhanced T1 mapping: MESA (multi-ethnic study of atherosclerosis). J Am Coll Cardiol 2013;62(14):1280–1287.
52. Look DC, Locker DR. Time saving in measurement of NMR and EPR relaxation times. Rev Sci Instrum 1970;41(2):250–251.
53. Messroghli DR, Greiser A, Fröhlich M, Dietz R, Schulz-Menger J. Optimization and validation of a fully-integrated pulse sequence for modified Look-Locker inversion-recovery (MOLLI) T1 mapping of the heart. J Magn Reson Imaging 2007;26(4): 1081–1086.
54. Messroghli DR, Radjenovic A, Kozerke S, Higgins DM, Sivananthan MU, Ridgway JP. Modified Look-Locker inversion recovery (MOLLI) for high-resolution T1 mapping of the heart. Magn Reson Med 2004;52(1):141–146.
55. Piechnik SK, Ferreira VM, Dall'Armellina E, et al. Shortened modified Look-Locker inversion recovery (ShMOLLI) for clinical myocardial T1-mapping at 1.5 and 3 T within a 9 heartbeat breathhold. J Cardiovasc Magn Reson 2010; 12:69.

56. Shi X, Kim SE, Jeong EK. Single-shot T1 mapping using simultaneous acquisitions of spin- and stimulated-echo-planar imaging (2D ss-SESTEPI). Magn Reson Med 2010;64(3):734–742.
57. Warntjes MJB, Kihlberg J, Engvall J. Rapid T1 quantification based on 3D phase sensitive inversion recovery. BMC Med Imaging 2010;10:19.
58. Been M, Thomson BJ, Smith MA, et al. Myocardial involvement in systemic lupus erythematosus detected by magnetic resonance imaging. Eur Heart J 1988;9(11):1250–1256.
59. Messroghli DR, Walters K, Plein S, et al. Myocardial T1 mapping: application to patients with acute and chronic myocardial infarction. Magn Reson Med 2007;58(1):34–40.
60. Xue H, Shah S, Greiser A, et al. Motion correction for myocardial T1 mapping using image registration with synthetic image estimation. Magn Reson Med 2012;67(6):1644–1655.
61. Ellims AH, Iles LM, Ling LH, Hare JL, Kaye DM, Taylor AJ. Diffuse myocardial fibrosis in hypertrophic cardiomyopathy can be identified by cardiovascular magnetic resonance and is associated with left ventricular diastolic dysfunction. J Cardiovasc Magn Reson 2012;14:76.
62. Marks B, Mitchell DG, Simelaro JP. Breath-holding in healthy and pulmonary-compromised populations: effects of hyperventilation and oxygen inspiration. J Magn Reson Imaging 1997;7(3):595–597.
63. Gai N, Turkbey EB, Nazarian S, et al. T1 mapping of the gadolinium-enhanced myocardium: adjustment for factors affecting interpatient comparison. Magn Reson Med 2011;65(5):1407–1415.
64. Lee JJ, Liu S, Nacif MS, et al. Myocardial T1 and extracellular volume fraction mapping at 3 tesla. J Cardiovasc Magn Reson 2011;13:75.
65. Broberg CS, Chugh SS, Conklin C, Sahn DJ, Jerosch-Herold M. Quantification of diffuse myocardial fibrosis and its association with myocardial dysfunction in congenital heart disease. Circ Cardiovasc Imaging 2010;3(6):727–734.
66. Kehr E, Sono M, Chugh SS, Jerosch-Herold M. Gadolinium-enhanced magnetic resonance imaging for detection and quantification of fibrosis in human myocardium in vitro. Int J Cardiovasc Imaging 2008;24(1):61–68.
67. Flett AS, Hayward MP, Ashworth MT, et al. Equilibrium contrast cardiovascular magnetic resonance for the measurement of diffuse myocardial fibrosis: preliminary validation in humans. Circulation 2010; 122(2):138–144.
68. Arheden H, Saeed M, Higgins CB, et al. Measurement of the distribution volume of gadopentetate dimeglumine at echo-planar MR imaging to quantify myocardial infarction: comparison with 99mTc-DTPA autoradiography in rats. Radiology 1999;211 (3):698–708.
69. Ugander M, Oki AJ, Hsu LY, et al. Extracellular volume imaging by magnetic resonance imaging provides insights into overt and sub-clinical myocardial pathology. Eur Heart J 2012;33(10):1268–1278.
70. Messroghli DR, Niendorf T, Schulz-Menger J, Dietz R, Friedrich MG. T1 mapping in patients with acute myocardial infarction. J Cardiovasc Magn Reson 2003;5(2):353–359.
71. Klein C, Nekolla SG, Balbach T, et al. The influence of myocardial blood flow and volume of distribution on late Gd-DTPA kinetics in ischemic heart failure. J Magn Reson Imaging 2004;20(4): 588–593.
72. Maceira AM, Joshi J, Prasad SK, et al. Cardiovascular magnetic resonance in cardiac amyloidosis. Circulation 2005;111(2):186–193.
73. Sparrow P, Messroghli DR, Reid S, Ridgway JP, Bainbridge G, Sivananthan MU. Myocardial T1 mapping for detection of left ventricular myocardial fibrosis in chronic aortic regurgitation: pilot study. AJR Am J Roentgenol 2006;187(6):W630–W635.
74. Hosch W, Bock M, Libicher M, et al. MR-relaxometry of myocardial tissue: significant elevation of T1 and T2 relaxation times in cardiac amyloidosis. Invest Radiol 2007;42(9):636–642.
75. Maceira AM, Prasad SK, Hawkins PN, Roughton M, Pennell DJ. Cardiovascular magnetic resonance and prognosis in cardiac amyloidosis. J Cardiovasc Magn Reson 2008;10:54.
76. Amano Y, Takayama M, Kumita S. Contrast-enhanced myocardial T1-weighted scout (Look-Locker) imaging for the detection of myocardial damages in hypertrophic cardiomyopathy. J Magn Reson Imaging 2009;30(4):778–784.
77. Jellis C, Wright J, Kennedy D, et al. Association of imaging markers of myocardial fibrosis with metabolic and functional disturbances in early diabetic cardiomyopathy. Circ Cardiovasc Imaging 2011;4 (6):693–702.
78. Ng ACT, Auger D, Delgado V, et al. Association between diffuse myocardial fibrosis by cardiac magnetic resonance contrast-enhanced T1 mapping and subclinical myocardial dysfunction in diabetic patients: a pilot study. Circ Cardiovasc Imaging 2012; 5(1):51–59.
79. Bauner KU, Biffar A, Theisen D, et al. Extracellular volume fractions in chronic myocardial infarction. Invest Radiol 2012;47(9):538–545.
80. Turkbey EB, Gai N, Lima JAC, et al. Assessment of cardiac involvement in myotonic muscular dystrophy by T1 mapping on magnetic resonance imaging. Heart Rhythm 2012;9(10):1691–1697.
81. Kellman P, Wilson JR, Xue H, et al. Extracellular volume fraction mapping in the myocardium. II. Initial clinical experience. J Cardiovasc Magn Reson 2012;14:64.
82. Ferreira VM, Piechnik SK, Dall'Armellina E, et al. Non-contrast T1-mapping detects acute myocardial edema with high diagnostic accuracy: a comparison to T2-weighted cardiovascular magnetic resonance. J Cardiovasc Magn Reson 2012;14:42.

RadioGraphics

Myocardial T1 Mapping: Techniques and Potential Applications

Jeremy R. Burt, MD • Stefan L. Zimmerman, MD • Ihab R. Kamel, MD, PhD • Marc Halushka, MD, PhD • David A. Bluemke, MD, PhD

RadioGraphics 2014; 34:377–395 • **Published online** 10.1148/rg.342125121 • **Content Codes:** CA MR

Page 377
Increased myocardial collagen deposition is the common endpoint for a wide variety of cardiomyopathies and results in abnormal myocardial stiffness and contractility, which leads to progression of heart failure and disruption of the intercellular communication grid and which, in turn, may lead to malignant arrhythmias and sudden death. Indeed, multiple clinical studies have shown fibrosis to be a major independent predictor of adverse cardiac outcomes (1–4).

Page 379
Ideally, an accurate noninvasive method would allow early detection of disease, accurate prognostication, and targeted guidance of treatment without the risks associated with invasive methods. Cardiac MR imaging has the potential to fulfill these criteria and provide a comprehensive cardiac assessment with detailed information about cardiac anatomy and function. In contrast to endomyocardial biopsy, sampling errors may be avoided with cardiac MR imaging by assessing the degree of fibrosis throughout the entire left ventricular myocardium.

Page 379
In some settings, the intrinsic T1 time of a tissue may act as a marker for the extent of myocardial disease (39,40). Specific IR-prepared cardiac MR imaging sequences are used to determine the rate of recovery of longitudinal magnetization (the T1 time).

Page 381
In animal and human studies, shortened T1 times in fibrotic myocardium on contrast-enhanced IR-prepared sequences showed good correlation with ex vivo fibrosis content (Fig 5) (39,43–46).

Page 392
Despite the diversity of these studies, a clear pattern is manifest: In general, postcontrast myocardial T1 relaxation times are shorter in patients with cardiac disease than they are in healthy control subjects.